energies

MDPI

Article

A Method for Estimating On-Field Photovoltaics System Efficiency Using Thermal Imaging and Weather Instrument Data and an Unmanned Aerial Vehicle

Wei-Hsiang Chiang [1], Han-Sheng Wu [1], Jong-Shinn Wu [2,*] and Shiow-Jyu Lin [3,*]

[1] College of Photonics, National Yang Ming Chiao Tung University, Tainan 71150, Taiwan
[2] Department of Mechanical Engineering, National Yang Ming Chiao Tung University, Hsinchu 30010, Taiwan
[3] Department of Electronic Engineering, National Ilan University, Ilan 260007, Taiwan
* Correspondence: chongsin@faculty.nctu.edu.tw (J.-S.W.); sjlin@niu.edu.tw (S.-J.L.); Tel.: +886-3-573-1693 (J.-S.W.); +886-3-935-7400 (S.-J.L.)

Abstract: A new approach is proposed for estimating the power efficiency of an on-field solar photovoltaics (PV) system using data from thermal imaging and weather instruments obtained using an unmanned aerial vehicle (UAV). This method is specifically designed for the non-intrusive detection of the performance of the PV system in a large-scale solar power plant that could be efficient, manpower saving, operationally safe and comprehensive. In this study, a drone instrumented with a radiometer, a thermometer and an anemometer flew at a height of 1.5 m with a maximum lateral flight speed of 3.6 m/s above the PV modules (60 cells each) with hotspots or with aging but without hotspots. The average temperatures of the PV modules were then calculated through the measured radiation intensity, ambient temperature and wind speed based on the published correlation formula. The experimental correlations were obtained by measuring over 60 aging PV modules without hot-spot damage, and the uncertainties of the estimated efficiencies fell between 2% and 5%. Through the use of 20 hot-spot damaged PV modules when the measured temperatures of the cells were in the range of 80–90 °C, it was found that based on the experimental correlationd, their power efficiencies would be lower than 40% if more than eight cells had hot spots in a PV module. By taking this simple measure, the operator can decide which PV module is damaged and should be replaced immediately. By taking such measures, one can reduce the loading effect of solar PV modules adjacent to them because of the low efficiency and high impedance caused by the damage. We believe the new approach developed in this study could be very cost-effective and time-saving for improving the efficiency of power plant operations.

Keywords: IR-imaging; outdoor testing; UAV detection; hotspots; cell efficiency

Citation: Chiang, W.-H.; Wu, H.-S.; Wu, J.-S.; Lin, S.-J. A Method for Estimating On-Field Photovoltaics System Efficiency Using Thermal Imaging and Weather Instrument Data and an Unmanned Aerial Vehicle. *Energies* **2022**, *15*, 5835. https://doi.org/10.3390/en15165835

Received: 29 June 2022
Accepted: 10 August 2022
Published: 11 August 2022

1. Introduction

Solar energy plays an increasingly important role in global energy production. According to the report published by IRENA in 2022, the world's renewable energy generation increased by 9.25% compared with 2020. Moreover, solar energy made up 854 GW of the total renewable energy supply in 2021, almost 10.7 times the 73 GW generated in 2011. China (307 GW), the USA (95 GW) and Japan (74 GW) [1] generate the most solar power in the world. Due to the dwindling supply of fossil fuels and global warming, the importance of solar power cannot be overemphasized.

The effectiveness of power generation using solar panels directly correlates with the production scale. In order to increase energy production, industrial companies usually lay out solar panels en masse. Unfortunately, throughout the lifetime of a solar panel, dust and other contaminants (such as bird droppings and debris) scatter and stick on their surfaces [2]. The solar panel cannot convert solar energy into electrical energy if it is not cleaned immediately. Instead, the solar energy converts to heat, causing hotspots [3] on

the solar panel and reducing its ability to generate electricity. Under ideal conditions, solar panels last approximately 25 years [4]. During their lifetime, their ability to generate power strongly depends on the quality of maintenance. Studying the power generation efficiency of installed solar panels by uninstalling and shipping them back to the factory is impractical.

There have been many previous studies using UAV with an IR imager to detect hotspots on solar panels. They can be classified into three kinds. The first is identifying the hotspots on a solar panel through image processing with the artificial neural network and classification learner algorithms [5–7]. The second is deriving the surface temperature of solar panels through the IR image and estimate the efficiency [8,9]. The third is identifying the solar panels with hotspots and pinpointing them with GPS coordinates and RGB images [10,11]. However, there seems to no study focusing on estimating the efficiency of solar panels with hotspots, which is the critical parameter that can decide if the panels should be replaced.

Current methods of analyzing solar panels include using ultrasound [12], thermal imaging [13–16] and electroluminescence (EL) imaging [17,18]. EL imaging analyzes the light emitted when forcing electricity through PV cells. As the emitted light correlates directly with the ion concentration in the PN junction of PV cells, analyzing the emitted light patterns allow engineers to study the integrity of the silicon in PV cells. The process is labor-intensive and time-consuming. Despite the outdoor EL imaging system developed by Mertens et al. [19] reducing some of the time and labor spent conducting analysis, it is still not entirely practical due to limitations on the operation environment. The most efficient examination method involves scanning the field of solar panels with an infrared (IR) camera mounted on a drone. However, this only provides a preliminary understanding of the hotspot distribution, as the thermal imagery cannot directly determine the module's power production efficiency [20]. The testing for these parameters still requires extensive manual labor.

A solar panel's surface temperature and appearance of hotspots directly affect its efficiency [21]. According to Refs. [22–24], the efficiency can be estimated based on the temperature of the modules. Fine et al. [25] proposed a method of estimating modular efficiency with an error of 4%. The other investigator [26] correlated the modular power and efficiency through measurements of long-term (one year) meteorological data. In addition, factors such as ambient temperature, wind velocity, and irradiance contribute to the change in surface temperature [27]. In order to conduct a real-time solar panel analysis of a solar power plant, this research developed an efficient, non-intrusive method of testing utilizing on-board IR imaging on drones with other instruments such as wind speed meter. We proposed the method of estimating the temperature of the modules through the instantaneous measured meteorological data. Then, through the correlation of the module efficiency with estimated temperature for different solar panel, one can still estimate the efficiency of the modules with an error of 2–5% based on the measured data presented in this study. The experiments conduct a preliminary analysis of solar panels using IR imaging and establish a relationship between power efficiency, temperature, and hotspots using regression, providing an additional method for analyzing solar panel efficiency in real-time.

2. Research Methods

A solar panel's energy output directly links to its efficiency. The analysis focuses on both thermal and electrical energy. Photovoltaic cells generate electricity using solar radiation. However, the photovoltaic cells also generate thermal energy through corresponding heat exchange processes. Therefore, both conventional contact measurements and contemporary non-contact methods such as IR imaging can estimate the performance of a photovoltaic cell.

Abnormal power generation causes anomalies to appear on the surfaces of solar panels. The influence of the presence of hotspots in the modules is well-known qualitatively, but

the quantitative effect of the number of hotspots on the efficiency of solar panels is rarely seen in the literature to the best of the authors' knowledge. In order to estimate a module's efficiency, this research compares the output of a brand-new solar panel, a solar panel with hotspot damage and temperature anomalies and a solar panel with temperature anomalies but no hotspots. Figure 1 presents the proposed process for analyzing the relationship between temperature and efficiency and the relationship between the number of hotspots and efficiency.

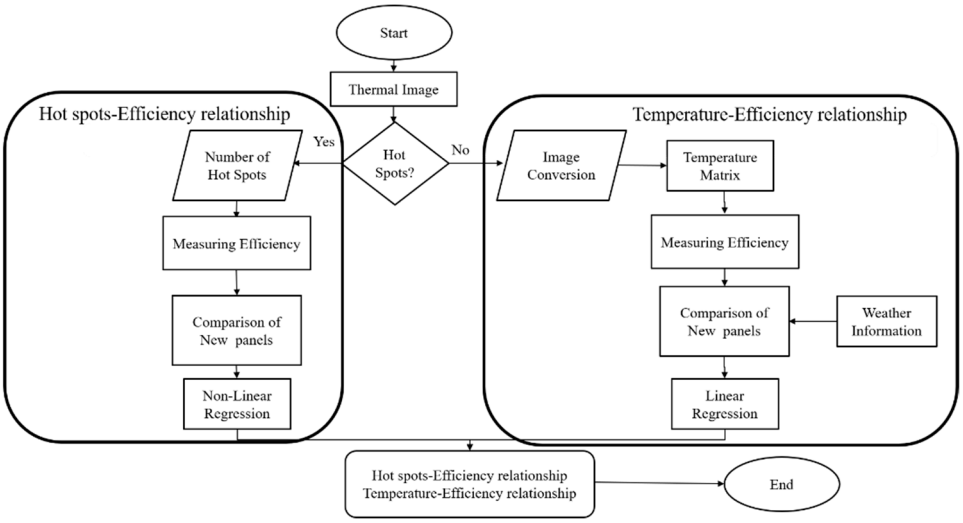

Figure 1. Proposed process of analyzing the relationships among the number of hotspots, temperature and efficiency.

2.1. Instrumentation

2.1.1. Unmanned Aerial Vehicle (UAV)

A quadcopter UAV (Model anafi thermal, Parrot) is used for taking thermal images of the solar panels. Due to its strong wind resistance, long operating distance, thermal image shooting, and advantages of custom flight and automatic shooting functions, it can be used for rapid detection at a large scale. Table 1 shows the specifications of the Parrot anafi thermal UAV. The moving speed and flying height of the UAV will affect the analysis of thermal images. In this study, in order to improve the detection efficiency and maintain its accuracy, the optimal flight speed and flight altitude were obtained by examining the measured data through multiple flight tests. They were found to be 3.6 m/s and 1.5 m respectively.

Table 1. Specifications of Parrot aniafi thermal UAV.

GNSS	GPS + GLONASS
Maximum transmission distance	4 KM
Maximum wind resistance	13.9 m/s
Maximum flight time	25 min
Size unfolded	242 × 315 × 64 mm
Weight	315 g
GNSS	GPS + GLONASS

2.1.2. Thermal Imager FLIR Lepton 3.5

The thermal imager used in this experiment was a FLIR Lepton 3.5 mounted on the Parrot anafi thermal UAV; the operation APP-FreeFlight 6 provided by Parrot enables it to directly use a mobile phone to monitor images remotely and perform photography. The IR imaging angle is always perpendicular to the modules through the attitude control of

the UAV. The tools provided by FLIR analyze the temperature and hotspot distribution of thermal photos. Table 2 shows the specifications of the thermal imager FLIR Lepton 3.5.

Table 2. Specification of FLIR Lepton 3.5.

Image Resolution	**160 × 120**
Heat sensitivity	<50 mK
Measurement range	−10–400 °C

2.1.3. HOBO Weather Station

The weather station of HOBO (Model RX2100, MicroRX) was used in this experiment. This weather station includes an air temperature and humidity probe, a wind speed sensor and an illuminance sensor. It can upload data to the cloud through 4G transmission, reaching one data point per minute. The measurement range of the air temperature and humidity probe was −40 °C to 75 °C at 0–100% RH, and the accuracy was ±0.21 °C and ±2.5% RH. The wind speed sensor is used to measure the instantaneous wind speed and the average wind speed and the maximum and minimum wind speed; the measurement unit is m/s. It has a measurement range of 0 to 76 m/s with an accuracy of ±1.1 m/s. The illuminance sensor is designed to measure the sun's luminosity with a measurement range of 0–1280 W/m^2, and an accuracy of ±10 W/m^2.

2.2. Temperature-Efficiency Relation

2.2.1. Module Temperature Calculation

We did not use Pt 100 for the validation of temperature measurements. We did use calibrated thermocouples (T type) for calibrating the temperatures measured by the IR thermal imaging. Through numerous measurements, we ensured that the measured temperatures between thermocouple and IR thermal imaging were within a difference of 0.3 °C as shown in Table 3. In order to obtain temperature readings from the thermal imager, first, input the image into a MATLAB code and then convert the 160 × 120 resolution thermal image into 19,200 greyscale values. The operator then manually selects the coordinates in need of analysis via commands. The FLIR tools then analyze the greyscale values of these coordinates and convert them into temperature values. Lastly, the software averages these temperature values to obtain the mean temperature of the selected area, as shown in Figure 2.

Table 3. Temperature comparison between thermocouple and thermal imaging.

Thermocouple	**Thermal Imaging**
33 °C	33 °C
46.8 °C	47 °C
55.3 °C	55 °C
62.7 °C	63 °C
71.2 °C	71 °C
84.9 °C	85 °C
88.7 °C	89 °C

2.2.2. Efficiency Estimation

Due to solar radiation not being constant throughout the day, this research instead focuses on photoelectric energy conversion efficiency. The power of the modules is calculated by measuring the current and voltage embedded in the inverter. In addition, it was also validated through the measurement by a handheld current groove meter. Dividing the output electrical power by the product of the solar radiation and the area of the module yields the conversion efficiency, as shown in Equation (1). Multiplying the measured output current by the output voltage yields the output power. Finally, dividing the quantity above by

the product of the instantaneous solar radiation and surface area (e.g., 1.611 m^2, SRCSolar XT-250P6B's solar panel rack) yields the conversion efficiency. Table 4 summarizes the related electrical properties and thermal coefficients of the SRCSolar (Model XT-250P6B).

$$\eta = \frac{P_{out}}{P_{in}} = \frac{P_{out}}{Solar\ radiation * Area} \quad (1)$$

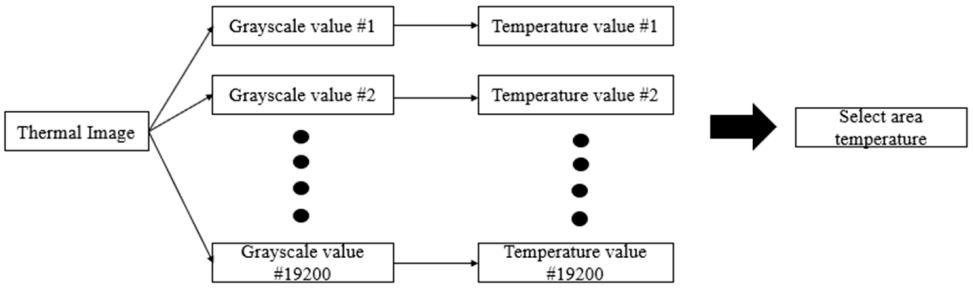

Figure 2. Regional temperature analysis.

Table 4. SRCSolar XT-250P6B's electrical properties and thermal coefficients.

P_{max}	250 W
I_{sc}	8.69 A
V_{oc}	37.40 V
I_{mp}	8.17 A
V_{mp}	30.60 V
Weight	18.5 kg
Dimension	1639 × 983 × 40 mm
NOCT	46 ± 2 °C
Thermal Coefficient of P_{max}	−0.44%/K
Thermal Coefficient of V_{oc}	−0.32%/K
Thermal Coefficient of I_{sc}	0.04%/K

2.2.3. Temperature Estimation of a Brand-New Module

External climate directly affects the operating temperature of a PV module. Additionally, lower ambient temperatures, higher solar radiation intensities and higher wind velocities directly correlate to increased solar panel efficiency [28]. There are two main methods of estimating a PV module's temperature distribution: steady state and unsteady. These two methods differ, as a steady-state method is time-independent, while specific parameters used in the unsteady-state method vary with time [28]. In order to study the instantaneous change in solar panel efficiency, this research utilizes the unsteady-state method.

Coskun et al. [29] summarized and tested various models used to analyze solar panel temperatures. This study used the models and compared them against the actual weather data. This research uses the modified approximation therein as:

$$T_c = T_a - 1.93666 + 0.0138 * G_T * (1 + 0.031 * T_a) * (1 - 0.042 * V_W) + 0.007882 * G_T - 0.0000134647 * {G_T}^2 \quad (2)$$

In the equation, T_c and T_a are the battery and ambient temperatures in Celcius, G_T is the solar radiation expressed in W/m^2 and V_W is the wind speed (m/s).

2.2.4. Linear Regression

This research obtains the temperature–efficiency relationship by first taking the temperature difference between a new solar panel and an old solar panel without hotspots and then analyzing their difference in efficiency via linear regression. The "old" modules are those that have been used for a while but for less than the lifetime limit of 20 years. They are certain to degrade after some use, but most of them are without hotspots. However, their temperatures are generally higher than the new modules during operation.

2.3. Hotspots-Efficiency Relationship

2.3.1. Analysis of the Number of Hotspots

The prolonged usage of solar panels outdoors causes aging and the appearance of hotspots. In addition, shading effects, micro-snail trail cracks and damaged surfaces cause hotspots to form on the surface of solar panels. Overheating hotspots on a solar panel cause safety hazards such as fire risks and electrical leakages. Unfortunately, the cost of replacing a solar panel whenever there is a hotspot is not economically viable for now.

This research categorizes hotspots into three categories according to their temperatures. Table 5 lists the proposed course of action for each hotspot category. Replace the solar panel immediately if the hotspot temperature is above 90 degrees. When the temperature us between 80 and 90 degrees, clean the panel and remove for inspection. As the temperature is between 50 and 80 degrees, perform cleaning of the solar panel and continue to monitor the hotspot's temperature. Categorizing hotspots and only replacing solar panels when it is necessary maximizes the yield of a solar power plant and minimizes unnecessary repair costs.

Table 5. The proposed course of action for each hotspot category.

Anomaly	Temperature	Course of Action
Level 1	Above 90 °C	Safety limit exceeded. Replace immediately
Level 2	80–90 °C	Clean the solar panel. Remove for inspection
Level 3	50–80 °C	Clean the solar panel. Continue monitoring

The hotspot number analysis is only for hotspots of 80–90 °C. Through MATLAB edge detection and the module temperature calculation method in the previous section, the number of hotspots existing in the thermal photo can be calculated. A typical example is shown in Figure 3.

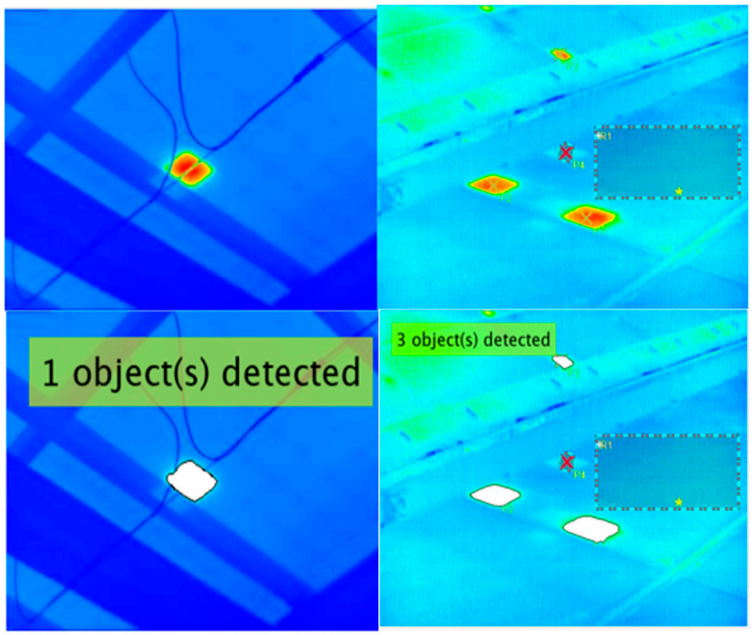

Figure 3. The images taken by an hand-held IR imager that were used to validate if the algorithm of image processing with edge detection can count the number of hotspots accurately.

2.3.2. Non-Linear Regression

In order to analyze the effects of hotspots on solar panel efficiency, this research uses the performance of a brand-new solar panel as the baseline. This research obtains

the hotspot–efficiency relationship by plotting the other data against the baseline using non-linear regression.

3. Results

3.1. Temperature Estimation of a Brand-New PV Module

Using Equation (2), Figure 4 compares the measured solar panel temperature against the estimated solar panel temperature. The figures show that the errors between the estimation and the measurement lie between 0.1% and 2.3%, which is impressive. Certain times throughout the day appear to possess larger errors. The study suggests that higher errors in solar panel hotspots between measurements and estimations may be attributed to the changes in solar radiation caused by the moving cloud during daytime. This result indicated that only steady weather conditions yield more accurate temperature estimations. However, even with the worst test case, the error is nevertheless small from a practical viewpoint.

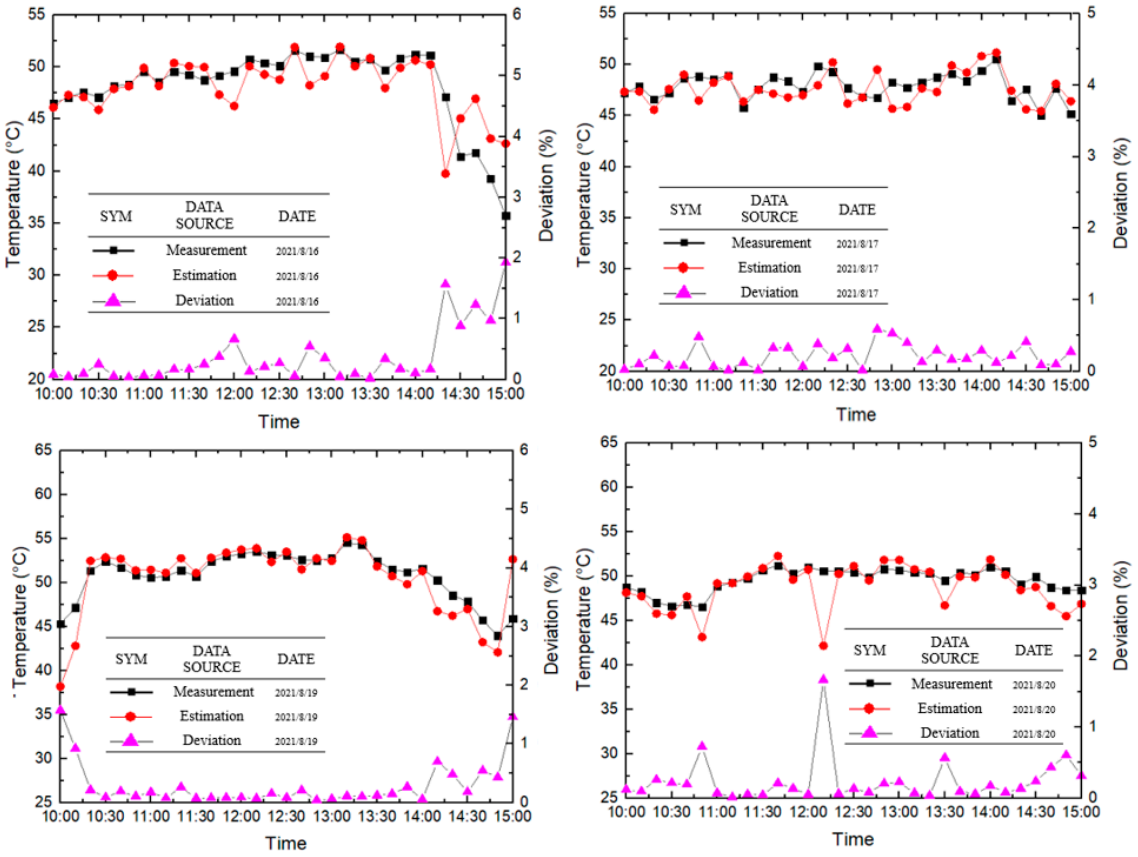

Figure 4. Temperature estimations of new photovoltaic panels on various days.

3.2. Data Analysis of Temperature-Efficiency Relations of Degraded PV Modules

The higher the surface temperatures of degraded solar panels are, the lower their efficiencies are. This research first estimates the surface temperatures of new solar panels and compares the results with degraded solar panels' efficiency and surface temperatures.

This research uses a thermal imager and a MATLAB program for estimating the module's instantaneous mean surface temperature and then compares these temperature data against a brand-new solar panel. This study studied 45 solar panels in total. Figure 5 presents the temperature–efficiency relationship (3) with an adjusted R-square of 0.95069 based on the experimental data listed in Table 6.

$$Eff_{new} - Eff_{old} = -0.03105 * (T_{new} - T_{old}) + 0.01599 \quad (3)$$

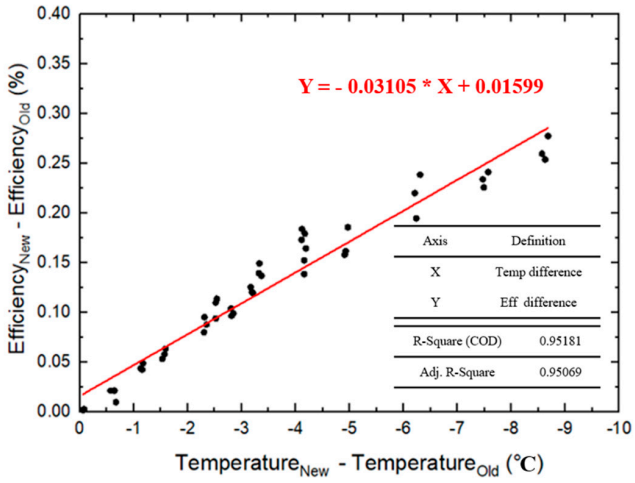

Figure 5. The temperature difference–efficiency difference correlation.

Table 6. Measured temperature–efficiency data.

Irradiance (W/m^2)	New Panel Temp (°C)	Old Panel Temp (°C)	Temp Difference (°C)	New Efficiency (%)	Old Efficiency (%)	Efficiency Difference (%)
461	43.68	43.73	−0.05	11.42255	11.4208	0.00175
1113	50.45	50.52	−0.07	10.37967	10.37761	0.00206
1096	52.51	52.59	−0.08	10.37807	10.37535	0.00272
921	48.79	49.36	−0.57	11.12735	11.10606	0.02129
892	49.49	50.13	−0.64	11.30102	11.27966	0.02136
924	51.07	51.74	−0.67	11.22055	11.21094	0.00961
768	45.33	46.46	−1.13	11.25393	11.21012	0.04381
866	49.56	50.72	−1.16	11.56103	11.51846	0.04257
668	43.6	44.77	−1.17	11.66763	11.61885	0.04878
843	50.86	52.39	−1.53	11.36721	11.3139	0.05331
753	51.04	52.61	−1.57	11.27779	11.21984	0.05795
806	49.34	50.93	−1.59	11.31042	11.24712	0.0633
923	49.77	52.07	−2.3	11.92728	11.84731	0.07997
868	46.21	48.52	−2.31	12.57884	12.48366	0.09518
903	49.43	51.78	−2.35	12.15666	12.06881	0.08785
643	47.95	50.47	−2.52	11.54196	11.43219	0.10977
853	51	53.52	−2.52	11.97723	11.8835	0.09373
636	46.39	48.93	−2.54	11.28913	11.17533	0.1138
759	50.54	53.34	−2.8	11.61759	11.51373	0.10386
779	50.86	53.67	−2.81	11.45176	11.35518	0.09658
836	48.59	51.44	−2.85	11.97583	11.87685	0.09898
809	46.14	49.31	−3.17	12.0874	11.96195	0.12545
311	36.17	39.36	−3.19	12.14819	12.02784	0.12035
522	42.87	46.08	−3.21	11.87632	11.75658	0.11974
943	50.07	53.39	−3.32	11.03679	10.89757	0.13922
918	51.02	54.35	−3.33	11.2053	11.05607	0.14923
828	53.05	56.42	−3.37	11.9386	11.80179	0.13681
772	45.25	49.36	−4.11	11.37902	11.20607	0.17295
896	48.75	52.87	−4.12	11.37894	11.19515	0.18379
959	50.89	55.05	−4.16	11.51876	11.38038	0.13838
952	47.46	51.62	−4.16	11.805	11.65282	0.15218
793	47.7	51.87	−4.17	11.08935	10.91018	0.17917
939	48.37	52.56	−4.19	11.74077	11.57643	0.16434
772	45.16	50.07	−4.91	11.52777	11.36994	0.15783
769	45.57	50.5	−4.93	11.4105	11.2489	0.1616
864	49.39	54.36	−4.97	11.40309	11.21751	0.18558
899	51.72	57.93	−6.21	11.61011	11.3902	0.21991
922	49.29	55.53	−6.24	11.23499	11.04042	0.19457
852	46.56	52.87	−6.31	11.97052	11.73213	0.23839
939	52.17	59.64	−7.47	10.96766	10.73385	0.23381
884	49.21	56.7	−7.49	11.01519	10.78951	0.22568
921	52.68	60.25	−7.57	11.11435	10.8732	0.24115
333	41.99	50.56	−8.57	11.08874	10.82908	0.25966
1004	48.68	57.31	−8.63	11.02406	10.77033	0.25373

Table 7 compares the results of the measured efficiency against the estimated efficiency calculated using Equation (3) with 15 degraded solar panels. The results show that the estimation errors lie within 2% to 5% of the measured efficiency that are reasonably accurate.

Table 7. Experimental results of efficiency estimation using the thermal imager onboard an UAV.

Irradiance (W/m^2)	$T_{New} - T_{Old}$(°C)	Estimated Efficiency (%)	Measured Efficiency (%)	Difference (%)
1043	−2.54	11.64282	11.41017	2.039
904	−1.18	11.26565	11.01086	2.314
883	−3.74	10.80313	11.07196	2.428
1019	−5.16	11.14723	10.86178	2.628
924	−2.24	10.61359	10.91159	2.731
834	−1.97	11.1353	11.46256	2.855
899	−4.31	11.22679	10.82215	3.739
1006	−4.68	11.34293	10.92378	3.837
1002	−3.22	11.74272	11.3039	3.882
872	−6.07	10.66328	11.1136	4.052
924	−1.38	11.38398	10.92859	4.167
956	−2.19	10.93736	10.47259	4.438
821	−3.54	11.59921	11.09569	4.538
1014	−3.14	11.28401	10.77099	4.763
979	−5.23	9.956334	10.46812	4.889

3.3. Analysis of Solar Panel Hotspots and Efficiency

This experiment captures images of solar panels with hotspots using thermal imagers and only studies hotspots with temperatures between 80 °C and 90 °C. After imaging the solar panels, a MATLAB code with edge detection algorithms computes the number of hotspots. Equation (1) then calculates the efficiency of the solar panel using the measured voltage and current output. Table 8 shows the efficiency data of twenty solar panels with hotspots. The collaborated power plant maintenance team believes that when the residual efficiency of a single solar panel is lower than 40%, the internal resistance of the overall tandem module may increase. It can result in a reduction in the power generation efficiency of the power plant. Therefore, in this study, photovoltaic modules with residual efficiency below 40% are determined to be replaced. Figure 6 yields the relationship between the number of hotspots and the solar panel's efficiency adjusted R-square of 0.9982 indicated by Equation (4).

$$\text{Residual Efficiency (\%)} = 41.332 + 58.668 \exp\left(-0.25387 * \text{Number of Hotspots}\right) \quad (4)$$

Table 8. Measured data of hotspot number and residual efficiency.

Irradiance (W/m^2)	Number of Hotspots	Efficiency without Hotspots (%)	Efficiency with Hotspots (%)	Efficiency Percentage Residual (%)
872	1	12.37	11.14	90.06
953	1	12.62	11.26	89.22
886	2	11.98	9.34	77.96
802	2	11.77	9.23	78.42
937	3	12.24	8.69	71
1004	3	12.65	8.87	70.12
999	4	12.61	8.07	64
967	4	12.49	8.01	64.13
941	5	12.27	7.24	59.01
977	5	12.43	7.32	58.89
1011	6	12.71	6.86	53.97
977	6	12.23	6.57	53.72
936	7	12.07	6.16	51.04
894	7	11.94	6.09	51.01
833	8	11.78	5.78	49.07

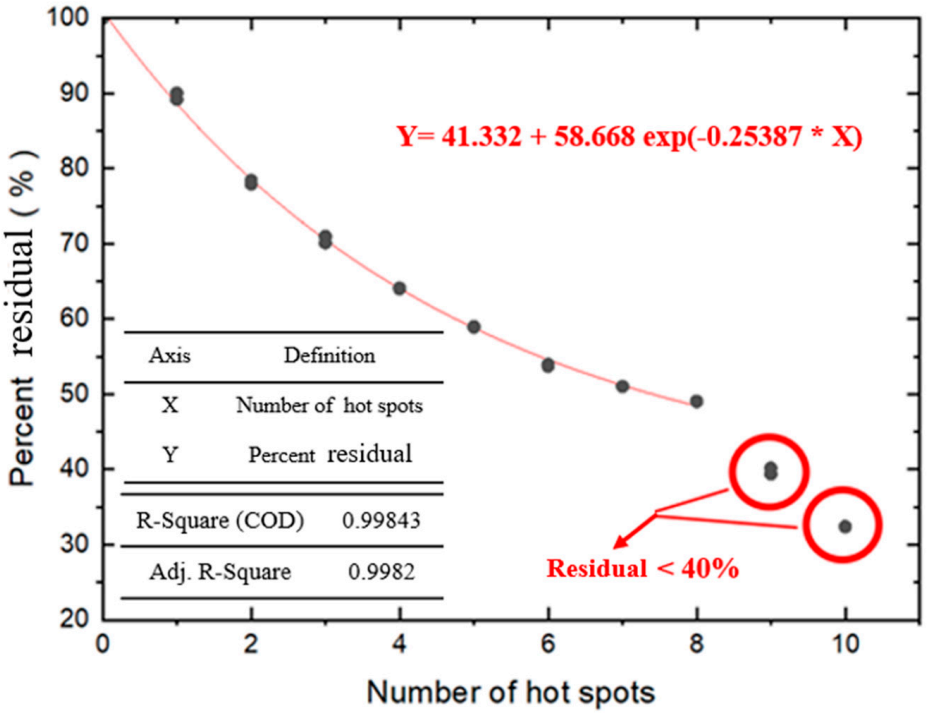

Figure 6. Hotspot number–residual efficiency correlation.

4. Conclusions

Usually, solar power plants of large surface areas are very challenging for inspection and maintenance at low cost. Removing solar panels to measure their efficiency requires a significant amount of time and manual effort. This research focuses on developing an efficient and reasonably accurate method of analyzing degraded solar panels and solar panels with hotspots using a combination of UAVs, thermal imagers and weather stations. The study estimates the efficiency by studying the effects of solar panel temperatures and the number of hotspots. The following summarizes the major findings of this study:

1. Under stable weather conditions, the solar panel temperature estimation equation developed by Coskun et al. [29] accurately estimates the temperature of a brand-new solar panel.
2. This research concludes that hotspots significantly decrease a solar panel's power output. In order to determine the relationship between the number of hotspots and the residual efficiency of a solar panel, this research studied 16 PV modules using a combination of a UAV and a thermal imager.
3. This research proposed a method specifically designed to estimate the residual efficiency of a degraded solar panel by comparing its performance with the temperature of a new solar panel using data from weather stations. Comparing the results of the estimated efficiency of new solar panels and 45 different degraded solar panels yielded a relationship between solar panel surface temperature and its efficiency. After investigating 15 solar panels, the measured errors lie within 2% and 5%.

5. Future Works

This research developed an efficient method of inspecting degrading solar panels and solar panels with hotspots. It also developed correlations with validations relating solar panel efficiencies to the number of hotspots and the surface temperatures of solar panels. In addition, aspects such as what type of damage is on the solar panel and the damage location deserve further investigation in the near future. Individual factors contributing to decreases in solar panel efficiency require further studies in the future. Results from these studies will contribute significantly to the analysis of solar panel deterioration.

Author Contributions: Methodology, J.-S.W.; Resources, J.-S.W.; Writing—original draft, W.-H.C. and H.-S.W.; Writing—review & editing, W.-H.C., J.-S.W. and S.-J.L. All authors have read and agreed to the published version of the manuscript.

Funding: This research received no external funding.

Informed Consent Statement: Not applicable.

Data Availability Statement: Not applicable.

Acknowledgments: The authors greatly appreciate BIG SUN Group, Taiwan, for providing solar panel field and technical assistance during this research.

Conflicts of Interest: The authors declare no conflict of interest.

References

1. IRENA. *Renewable Energy Statistics*; IRENA: Abu Dhabi, United Arab Emirates, 2022.
2. Matusz-Kalász, D.; Bodnár, I. Operation Problems of Solar Panel Caused by the Surface Contamination. *Energies* **2021**, *14*, 5461. [CrossRef]
3. Simon, M.; Meyer, E.L. Detection and analysis of hot-spot formation in solar cells. *Sol. Energy Mater. Sol. Cells* **2010**, *94*, 106–113. [CrossRef]
4. Tsanakas, J.A.; Karoglou, M.; Delegou, E.T.; Botsaris, P.N.; Bakolas, A.; Moropoulou, A. Assessment of the performance and defect investigation of PV modules after accelerated ageing tests. *Renew. Energy Power Qual. J.* **2013**, *1*, 866–872. [CrossRef]
5. Herraiz, Á.H.; Marugán, A.P.; Márquez, F.P.G. Photovoltaic plant condition monitoring using thermal images analysis by convolutional neural network-based structure. *Renew. Energy* **2020**, *153*, 334–348. [CrossRef]
6. Segovia Ramirez, I.; Das, B.; Garcia Marquez, F.P. Fault detection and diagnosis in photovoltaic panels by radiometric sensors embedded in unmanned aerial vehicles. *Prog. Photovolt.* **2022**, *30*, 240–256. [CrossRef]
7. Menéndez, O.; Guamán, R.; Pérez, M.; Auat Cheein, F. Photovoltaic Modules Diagnosis Using Artificial Vision Techniques for Artifact Minimization. *Energies* **2018**, *11*, 1688. [CrossRef]
8. Peng, Z.; Herfatmanesh, M.R.; Liu, Y. Cooled solar PV panels for output energy efficiency optimisation. *Energy Convers. Manag.* **2017**, *150*, 949–955. [CrossRef]
9. Amelia, A.R.; Irwan, Y.M.; Leow, W.Z.; Irwanto, M.; Safwati, I.; Zhafarina, M. Investigation of the Effect Temperature on Photovoltaic (PV) Panel Output Performance. *Int. J. Adv. Sci. Eng. Inf. Technol.* **2016**, *6*, 682–688.
10. Lee, D.H.; Park, J.H. Developing inspection methodology of solar energy plants by thermal infrared sensor on board unmanned aerial vehicles. *Energies* **2019**, *12*, 2928. [CrossRef]
11. Elidrissi, H.; Achakir, H.; Zefri, Y.; Sebari, I.; Aniba, G.; Hajji, H. Automatic on Field Detection and Localization of Defective Solar Photovoltaic Modules from Orthorectified RGB UAV Imagery. In Proceedings of the 2022 6th International Conference on Green Energy and Applications (ICGEA), Singapore, 4–6 March 2022; pp. 46–50.
12. Dallas, W.; Polupan, O.; Ostapenko, S. Resonance ultrasonic vibrations for crack detection in photovoltaic silicon wafers. *Meas. Sci. Technol.* **2007**, *18*, 852. [CrossRef]
13. Botsaris, P.N.; Tsanakas, J.A. Infrared thermography as an estimator technique of a photovoltaic module performance via operating temperature measurements. In Proceedings of the 10th European Conference on Non-Destructive Testing, Moscow, Russia, 7–11 June 2010.
14. Spagnolo, G.S.; Del Vecchio, P.; Makary, G.; Papalillo, D.; Martocchia, A. A review of IR thermography applied to PV systems. In Proceedings of the 2012 11th International Conference on Environment and Electrical Engineering, Venice, Italy, 18–25 May 2012; pp. 879–884.
15. Breitenstein, O.; Rakotoniaina, J.P.; Kaes, M.; Seren, S.; Pernau, T.; Hahn, G.; Isenberg, J. Lock-in thermography—A universal tool for local analysis of solar cells. In Proceedings of the 20th European Photovoltaic Solar Energy Conference, Barcelona, Spain, 6–10 June 2005; Volume 7, pp. 956–963.
16. Tsanakas, J.A.; Ha, L.; Buerhop, C. Faults and infrared thermographic diagnosis in operating c-Si photovoltaic modules: A review of research and future challenges. *Renew. Sustain. Energy Rev.* **2016**, *62*, 695–709. [CrossRef]
17. Kasemann, M.; Schubert, M.C.; The, M.; Köber, M.; Hermle, M.; Warta, W. Comparison of luminescence imaging and illuminated lock-in thermography on silicon solar cells. *Appl. Phys. Lett.* **2006**, *89*, 224102. [CrossRef]
18. Fuyuki, T.; Kondo, H.; Yamazaki, T.; Takahashi, Y.; Uraoka, Y. Photographic surveying of minority carrier diffusion length in polycrystalline silicon solar cells by electroluminescence. *Appl. Phys. Lett.* **2005**, *86*, 262108. [CrossRef]
19. Mertens, K.; Kösters, H.; Diehl, M. Low-cost-outdoor-EL: Cost-efficient extensive on-site quality analysis of solar modules. In Proceedings of the 31st European Photovoltaic Solar Energy Conference and Exhibition, Hamburg, Germany, 14–18 September 2015.
20. Grimaccia, F.; Leva, S.; Niccolai, A. PV plant digital mapping for modules' defects detection by unmanned aerial vehicles. *IET Renew. Power Gener.* **2017**, *11*, 1221–1228. [CrossRef]
21. Meneses-Rodríguez, D.; Horley, P.P.; Gonzalez-Hernandez, J.; Vorobiev, Y.V.; Gorley, P.N. Photovoltaic solar cells performance at elevated temperatures. *Sol. Energy* **2005**, *78*, 243–250. [CrossRef]

22. Khordehgah, N.; Guichet, V.; Lester, L.P.; Jouhara, H. Computational study and experimental validation of a solar photovoltaics and thermal technology. *Renew. Energy* **2019**, *143*, 1348–1356. [CrossRef]
23. Fu, H.; Li, G.; Li, F. Performance comparison of photovoltaic/thermal solar water heating systems with direct-coupled photovoltaic pump, traditional pump and natural circulation. *Renew Energy* **2019**, *136*, 463–472. [CrossRef]
24. Yadav, K.; Kumar, A.; Sastry, O.S.; Wandhare, R. Solar photovoltaics pumps operating head selection for the optimum efficiency. *Renew. Energy* **2019**, *134*, 169–177. [CrossRef]
25. Fine, J.P.; Dworkin, S.B.; Friedman, J. A methodology for predicting hybrid solar panel performance in different operating modes. *Renew. Energy* **2019**, *130*, 1198–1206. [CrossRef]
26. Ba, M.; Ramenah, H.; Tanougast, C. Forseeing energy photovoltaic output determination by a statistical model using real module temperature in the north east of France. *Renew. Energy* **2018**, *119*, 935–948. [CrossRef]
27. Dhimish, M. Defining the best-fit machine learning classifier to early diagnose photovoltaic solar cells hot-spots. *Case Stud. Therm. Eng.* **2021**, *25*, 100980. [CrossRef]
28. Hasan, M.A.; Sumathy, K. Photovoltaic thermal module concepts and their performance analysis: A review. *Renew. Sustain. Energy Rev.* **2010**, *14*, 1845–1859. [CrossRef]
29. Coskun, C.; Toygar, U.; Sarpdag, O.; Oktay, Z. Sensitivity analysis of implicit correlations for photovoltaic module temperature: A review. *J. Clean. Prod.* **2017**, *164*, 1474–1485. [CrossRef]